2014 IEEE International Conference on Robotics & Automation (ICRA)
Hong Kong Convention and Exhibition Center
May 31 - June 7, 2014. Hong Kong, China

Planar Fabrication of a Mesoscale Voice Coil Actuator

Benjamin Goldberg, Michael Karpelson, Onur Ozcan, and Robert J. Wood
Harvard University, School of Engineering and Applied Sciences, Cambridge, MA, USA

***Abstract*— Mesoscale robots are devices with characteristic dimensions in the centimeter to millimeter scale, with feature sizes ranging from millimeters to micrometers. Due to the physics involved in scaling down conventional motors, such robots frequently require novel approaches to actuation. Actuation can have a very significant effect on robot performance, particularly at small scales where locomotion becomes energetically expensive; however, existing options for small-scale actuation are quite limited. We present a mesoscale voice coil actuator (VCA) with favorable scaling characteristics and a design that minimizes costly frictional effects at small scales while allowing fast, linear, high-displacement motion. The VCA is fabricated using planar manufacturing techniques, making it well-suited for integration into a number of mesoscale robotic platforms and for mass production. The designed VCA has a mass of 310mg, maximum force of 11.8mN, bandwidth of 51Hz, and a stroke of 4mm.**

I. INTRODUCTION

Lorentz forces are the basis for many of the common actuation methods in robotics. Actuators based on Lorentz forces provide relatively large forces, torques, and energy and power densities ($\sim 1\text{kW}\,\text{kg}^{-1}$[1]). DC motors, in particular, are compact, easy to operate, and robust. As device scale is reduced, however, frictional forces begin to dominate over the electromagnetic force produced by the motor. For example, a 190mg Namiki brushless motor has a power density of only $39\text{W}\,\text{kg}^{-1}$ [2], compared to $658\text{W}\,\text{kg}^{-1}$ for a 730g brushless motor [1]. Moreover, interfacing such motors with typical loads encountered in mesoscale robotic platforms necessitates additional gearing and transmission mechanisms, which further reduce efficiency and power density. This has led to interest in other methods of actuation suitable for mesoscale robotics, including electrostatic [3] [4], piezoelectric [5] [6], or thermal expansion [7] [8].

Actuation choices in mesoscale robotics are limited in capabilities and ease of integration. Piezoelectric actuators compensate for low energy densities ($\sim 2.35\ \text{J}\,\text{kg}^{-1}$)[9] with high bandwidths for high frequency cyclic power delivery or precision motion. Successful examples include actuators in a micro gripper [5], quadrupeds [6] [10], and a flying robotic insect [11]. However, piezoelectric actuators typically produce low strokes, are composed of dense, lead-based brittle ceramics, and require high operating voltages (tens to hundreds of volts). Furthermore, these high operating voltages can reduce the effective energy and power densities by requiring additional drive electronics. Millimeter-scale shape memory and electroactive polymer actuators leverage large energy densities ($\sim 15\ \text{kJ}\,\text{kg}^{-1}$ and $\sim 23\text{kJ}\,\text{kg}^{-1}$, respectively [12]) but with very low efficiency and bandwidth.

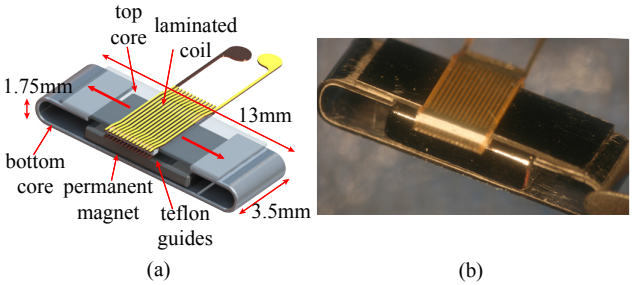

Fig. 1. (a) Design of the voice coil actuator, (b) the manufactured prototype.

Here, we present a compact Voice Coil Actuator (VCA) design as shown in Fig. 1. Voice coil actuation is a well-known technology used in many positioning applications (e.g. lateral positioning of hard drive heads, vertical positioning of focusing lens in CD and DVD drives). VCAs offer large, configurable displacements and linear output with simple drive electronics, making them an attractive alternative to piezoelectric actuators for mesoscale robotics. For example, VCAs can reduce transmission complexity in mesoscale robot designs where a high-stroke linear output is desired. Furthermore, VCAs used in control applications may not need high power density, just suitable position control and bandwidth. On the downside, VCAs are typically assembled using conventional manufacturing processes, which increases the difficulty and cost of integrating them into mesoscale robots. Examples of VCAs at this scale require tedious hand fabrication, and have either non-linear outputs or high friction [13] [14] [15].

Here, fabrication of the VCA relies primarily on planar manufacturing techniques, making it ideal for integration into mechanisms fabricated using lamination, folding, and the recently developed Pop-up book MEMS techniques [16]. Pop-up book MEMS is a novel fabrication process capable of creating complex millimeter-scale articulated structures via bulk machining, lamination, and assembly by folding. Previously, piezoelectric actuators developed by Wood et al. [9] had been integrated into these structures. However, such actuators are not ideal for all applications, and the integration of compact electromagnetic actuators into such a process greatly increases its potential in biomedical, microrobotic, optical, and other applications. The contribution of this work is the design and scaling analysis for a mesoscale VCA, manufacturing methods to create the VCA, and characterization and comparison to other mesoscale actuators.

This paper discusses design and fabrication of a compact

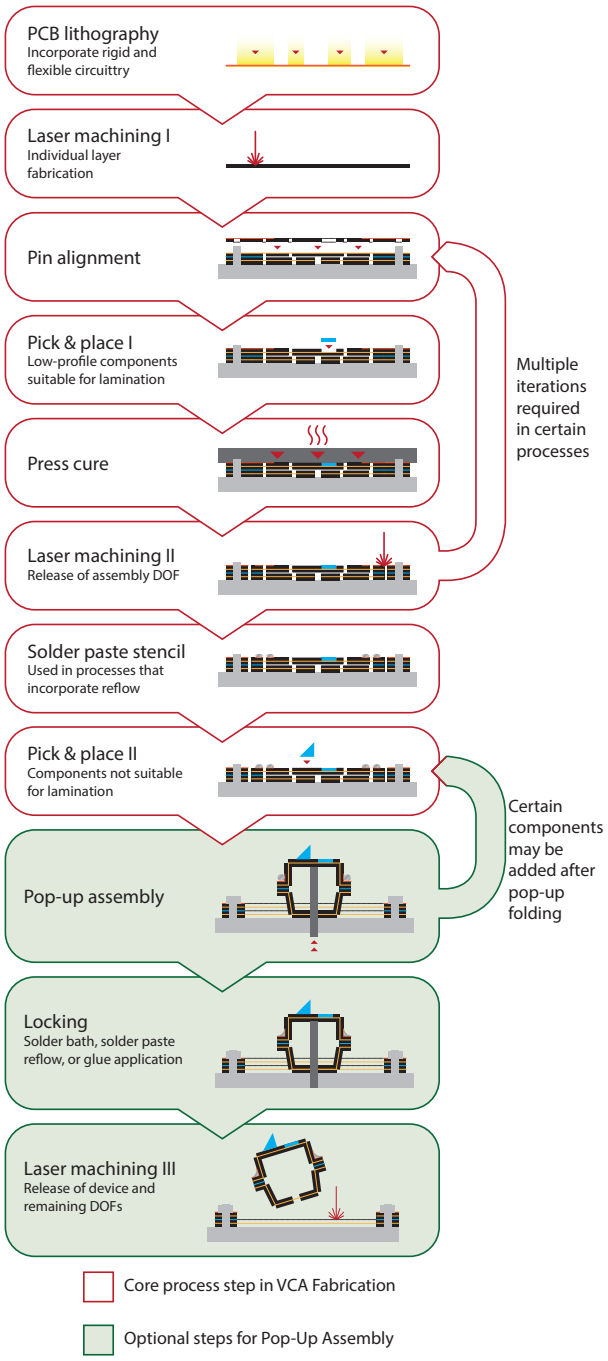

Fig. 2. PC-MEMS process workflow.

VCA (Section II), scaling laws (Section III), modeling (Section IV), and experimental results (Section VI), including electrical and mechanical properties of the VCA prototype, and the evaluation of various performance metrics such as displacement, force, frequency, size, mass, and input electrical power.

II. DESIGN AND FABRICATION

A. Design

The VCA is composed of three main parts: a laminated coil fabricated using planar methods, a permalloy core, and an N42 Nedodymium rare earth magnet as seen in Fig. 1. The coil surrounds the top part of the core and is free to translate linearly in either direction upon interaction of current in the coil and the magnetic field produced by the permanent magnet. By reversing the direction of current in the coil, motion in both directions is possible. The overall size of the actuator is $13\times3.5\times1.75$mm, and mass is 310mg. The coil consists of a top and bottom flexible circuit with patterned traces and has a turn ratio of five turns/mm with a total of 21 turns.

There are numerous design parameters which affect the performance of the actuator. Here, we focus on: Core material, core geometry, coil turn density, coil length, coil guide materials, and magnet geometry. These design parameters are addressed in more detail in section IV.

B. Pop-up Book MEMS Fabrication

The VCA is comprised of several different material layers and the fabrication process follows the pop-up book MEMS process workflow shown in Fig. 2.

The PC-MEMS process for constructing the VCA incorporates various stages of PCB lithography, laser machining, adhesive curing, pick and place assembly, solder reflow, and assembly by folding. The magnetic coil of the VCA consists of the six layers indicated in Fig. 3 and surrounds the top part of the VCA core.

The coil winding consists of copper traces on a flexible polyimide substrate (single-sided Pyralux®AC 182500R). The traces on the top and bottom layers, as seen in Fig. 3, are patterned in a PCB lithography process and laser machined to align with other layers of the laminate. The top traces are angled in order to form a single winding when connected to the straight bottom traces. Before lamination, the copper traces are pre-tinned with solder for reflow during final processing. The bottom flex-circuit and plastic spacer layers are shown on the alignment jig in Fig. 4a. The rest of the layers in Fig. 3 are stacked together on the alignment jig (Fig. 4b-d) and cured under heat and pressure. The resulting laminate is shown in Fig. 4e. Next, the solder is reflowed to electrically connect the top and bottom traces. A final laser machining release cut separates the coil and top core assembly from the sacrificial alignment features. The characteristics of the fabricated coil are listed in Table I.

TABLE I
SUMMARY OF PLANAR VCA SPECIFICATIONS

Overall Mass	310mg
Magnet Mass	115mg
Coil Mass	16mg
Number of turns	21
Coil Length	4.2mm
Wire Cross Sectional Area	1440μ m^2
Coil Resistance	6.0Ω

Planar fabrication of the coil opens the ability to incorporate other mechanical linkages and structures. For example, a linear bearing can be introduced, as in Fig. 5; the bearing

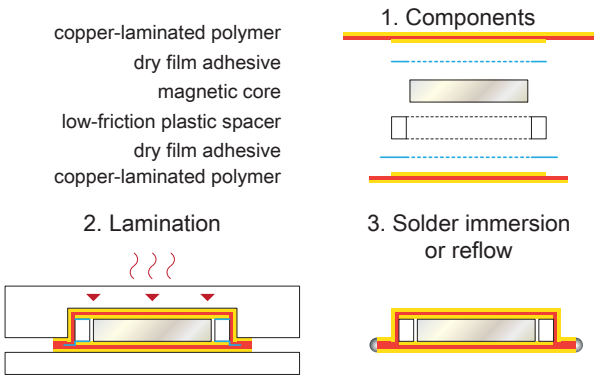

Fig. 3. Layers of the coil laminate.

uses flexible polyimide layers to form rotary joints that constrain the motion of the coil and eliminate any contact between the coil and core during actuation. Such structures can be manufactured concurrently with other pop-up book MEMS components to interface with robot transmissions and create complex geometries and kinematics. For example, a transmission can be directly connected to the guide rails of the sarrus linkage (Fig. 5). In section VI, we present results that include a spring element representing such a linear bearing.

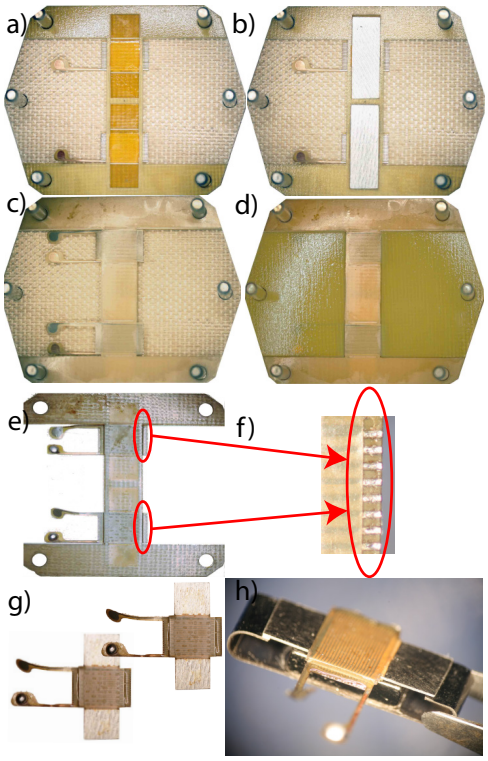

Fig. 4. (a) Bottom traces and teflon guides. (b) Metal core inserted between guides. (c) Top traces placed over teflon. (d) Teflon jig inserted to compress top and bottom traces together. (e) Traces reflowed under heat and pressure. (f) Close up of reflowed traces. (g) Coil and top core released from support material. (h) Top core placed on top of bottom core and permanent magnet.

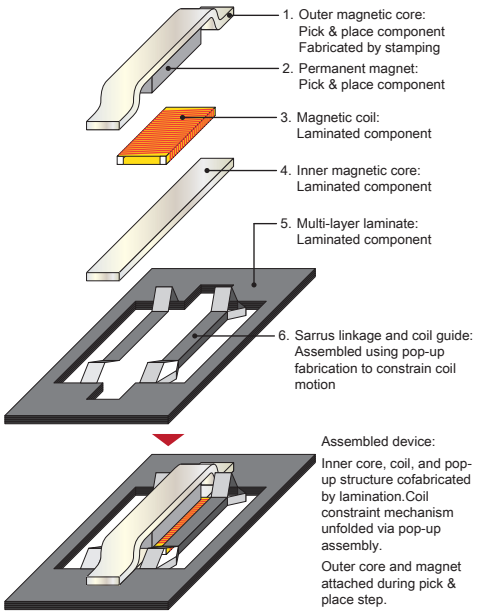

Fig. 5. A design that incorporates a flexure-based linear bearing to constrain coil motion, eliminating friction between the coil and the core.

III. SCALING ANALYSIS

The scaling relationship between actuators with similar properties can be expressed by a single variable, s, representing the characteristic length of the actuator. Force, mass, and acceleration vary with s and indicate the scaling effect on performance. For example, mass is proportional to s^3 which implies that when the scale decreases by a factor of 10, mass is reduced by 10^3.

The proposed VCA follows the Lorentz force law for a current-carrying loop,

$$F_L = kLN\vec{i} \times \vec{B} \tag{1}$$

where k is a constant of proportionality, L is the length of the coil, N is the number of turns in the coil, $\vec{i}$ is the current in the coil, and $\vec{B}$ is the magnetic field of a permanent magnet. Each parameter in Eq. 1 has a known scaling law for the characteristic length scale, s, and combines to yield the Lorentz force scaling of s^3.

$$F_L \propto s^0 s^1 s^0 s^2 \times s^0 \Rightarrow F_L \propto s^3 \tag{2}$$

Note that current, $\vec{i}$, scales as s^2 under the assumption of constant current density, the magnetic field, $\vec{B}$, of a permanent magnet is assumed to be a material property that is scale independent, and the number of turns, N, is scale independent under the assumption of scaling wire diameter with coil length (i.e. a smaller coil will contain a smaller diameter wire).

While the Lorentz force for a conventional DC motor has the same scaling behavior, the net force is dominated by frictional effects (s^2) in the bearings and pin joints inherent in a rotational motor design. In the VCA design presented

here, flexure-based mechanisms can completely eliminate the need for conventional bearings or pin joints.

In addition to force, performance metrics considered in this analysis include the mass, bandwidth, displacement, work, power, force density, energy density, power density, and efficiency of the actuator. For example, mass is proportional to volume (s^3), while stroke is proportional to length(s^1). Efficiency is illustrative of how the other scaling laws are obtained and is defined as follows:

$$\eta = \frac{\text{Power Out}}{\text{Power In}} = \frac{\text{Force}\times\text{Stroke}\times\text{Bandwidth}}{\text{Current}^2\times\text{Resistance}}$$

$$\eta \propto \frac{s^3 s^1 s^{-0.5}}{(s^2)^2 s^{-1}} = s^{0.5} \tag{3}$$

Table II summarizes the results of this scaling analysis for each of the performance metrics where 'density' indicates a per mass metric.

TABLE II
PERFORMANCE METRIC SCALING ANALYSIS FOR VCA

Mass	s^3	Energy Output	s^4
Force	s^3	Power Output	$s^{3.5}$
Stroke	s^1	Force Density	s^0
Bandwidth[17]	$s^{-0.5}$	Energy Density	s^1
Efficiency	$s^{0.5}$	Power Density	$s^{0.5}$
Resistance	s^{-1}		

While the force scaling as s^3 results in a large penalty as a design is scaled down, mass also scales as s^3, so the force density of the actuator should be scale invariant. Bandwidth scales as $s^{-0.5}$ indicating the potential for faster actuation at smaller scales. The increase in bandwidth results in only a small decrease in the power density ($s^{0.5}$) as the design is scaled down.

IV. MODELING

A. Static Model

Estimates of actuator performance are obtained using COMSOL Multiphysics® simulation software. This simulation is helpful in visualizing the lines of magnetic flux in order to maximize the magnetic field in the vicinity of the coil and in obtaining estimates of resulting forces. The permanent magnet has a nominal coercive force of 900kA m^{-1} (K & J Magnetics B4201 [18]) and geometries and materials match those described in section II. The simulated static force on the coil with 0.5 A current is 15.6mN. Results of the simulation are shown in Fig. 6 and are related to the prototype VCA in section VI.

Here, displacement is a simple geometric limitation. Additionally, mass of the coil is an order of magnitude less than the rest of the actuator, leaving little room for improvement in bandwidth. Therefore, we wish to maximize the force output. The design space in section II includes parameters such as coil turn density, coil length, and coil current which all have linear effects on produced force. The effect of these parameters can be easily obtained without a computer model. Other parameters that have an effect on static force include core geometry, material selection and magnet geometry. Selection of these parameters is guided by the computer model resulting in the chosen lengths, geometries, and materials presented in Fig. 1 and Table I.

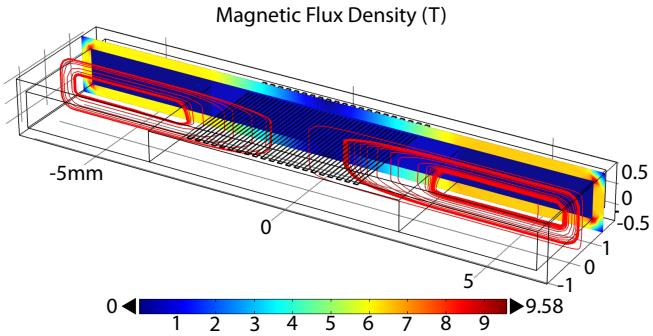

Fig. 6. COMSOL simulation of magnetic flux in the VCA.

B. Dynamic Model

The dynamic performance of the VCA is modeled as a time dependent mass-spring-damper system with coupling between the mechanical and electrical parameters. Friction is neglected in the dynamic model with the addition of the linear bearing described in section V. The mechanical model is:

$$\frac{d^2x}{dt^2} = \frac{F_L - b\frac{dx}{dt} - k_s x}{m} \tag{4}$$

where F_L is the Lorentz force, x is position, k_s is the spring constant of a transmission or linear bearing, and m is the mass of the coil. The electrical model is:

$$\frac{di}{dt} = \frac{k_c\frac{dx}{dt} + iR - V_{in}}{L} \tag{5}$$

where i is the current in the coil, k_c is a back-EMF constant, R is the resistance of the coil, V_{in} is the applied voltage to the coil, and L is the inductance of the coil.

From Eqs. 4 and 5, the overall system transfer function is:

$$\frac{X(s)}{V_{in}(s)} = \frac{A}{mLs^3 + (bL+mR)s^2 + (Lk_s + Rb + k_c A)s + Rk_s} \tag{6}$$

where $A = kLBN$ is from Eq. 1, assuming the current in the coil and the magnetic field are perpendicular.

V. EXPERIMENTAL SETUP

The VCA is controlled through MATLAB using custom drive electronics and a data acquisition card (NI DAQ-6008). Custom waveforms are generated in MATLAB and sent to the VCA to generate currents between -1.2A and 1.2A at a maximum power of 15W. Typical operating conditions for the VCA are 4.0V at 0.4A. The custom force sensor is a single degree of freedom, capacitive force sensor from [19] and is interfaced to MATLAB through a signal conditioning box (PISeca E-852) and the DAQ. Displacement data is collected

using a high speed camera (Vision Research Phantom V7.3) and automated video tracking software (Xcitex ProAnalyst). A picture of the experimental setup appears in Fig. 7.

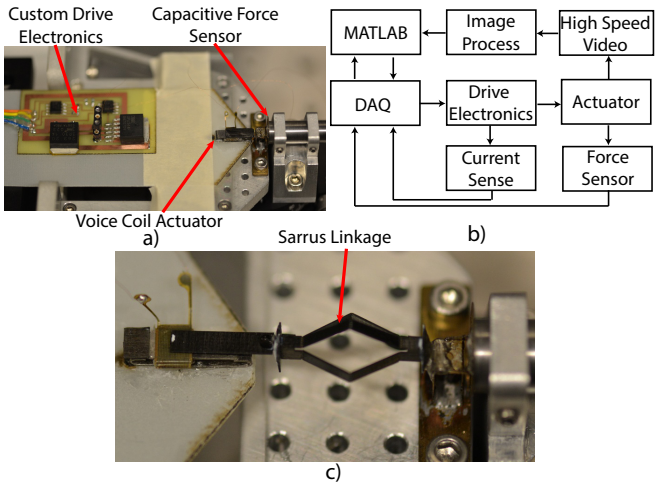

Fig. 7. a) Experimental setup with VCA, custom drive electronics, and force sensor. b) Block diagram of experimental setup. c) Experimental setup with sarrus linkage element.

Performance of the VCA is measured in two configurations; one configuration with no additional spring element to measure blocked force, and a second configuration with an additional spring element to validate the dynamic model. In the first case the actuator setup is configured as in Fig. 7a. Blocked force is measured without a sarrus linkage spring element in order to eliminate the need to preload or perfectly tune the spring element such that the actuator does not reach the limits of displacement at all currents but still allows appreciable coil motion in the frequency analysis. In the first configuration, measurements are taken both quasi-statically with step inputs and dynamically with a current input that increases linearly in frequency. This configuration is used to obtain the performance metrics listed in section VI-A.

In the second case, the dynamic response of the actuator is measured with a spring element, as in Fig. 7c. In this configuration, the spring element is a flexure-based sarrus linkage that suspends the coil around the central core. The sarrus linkage acts a linear bearing and eliminates contact between the coil and core. In the model, this element is assumed to eliminate all friction acting on the coil. Future designs can incorporate such a linear bearing internal to the structure of the actuator, as in Fig. 5.

Additionally, a VCA with a hand-wound coil is constructed to compare the performance of planar and hand fabrication. The hand wound coil consists of 100 turns of 43AWG wire with all other core elements remaining the same.

VI. RESULTS

A. Power Output Measurements

The quasi-static force measurements for the planar VCA, hand-wound VCA, and the COMSOL model are shown in Fig. 8. The fits for all of the data follow the linear Lorentz force relationship $\frac{F}{N} = k\vec{i} \times \vec{B}$. The negative y-intercept of the experimental data indicates the effect of static friction on the coil. In the planar VCA, the static friction is 3.03mN and in the hand wound VCA, the static friction is 16.4mN. A lower static friction in the planar coil can be attributed to improved tolerances, lower-friction materials, and less contact area on the sides of the core section enclosed by the winding. The corresponding slopes of the planar and hand wound VCA indicate little difference in normalized force output between the two methods of creating the coil. The benefit of the hand wound coil is a very high turn density. An insulated wire coil can be wound arbitrarily close together and on multiple layers, whereas the planar coil is limited in the current iteration of the manufacturing process to a single layer with a turn density of approximately five turns per millimeter since higher turn ratios make it difficult to reliably join the two halves of the winding. Benefits of the planar coil are planar fabrication and reduced friction. The COMSOL model predicts a higher actuator force since it does not account for friction, and is considered an upper bound for actuator output of the current geometry.

Performance measurements for the planar coil and hand wound coil are summarized in Table III. The maximum force for the planar coil is 11.8mN at a current of 0.6A compared to 59.6mN at 0.75A for the hand-wound coil. The resulting power density for the planar coil VCA and hand-wound VCA are 1.95W kg^{-1} and 6.97W kg^{-1}, respectively. This corresponds to 92.8mW kg^{-1} per turn for the planar coil and 69.7mW kg^{-1} per turn for the hand-wound coil. On a per turn basis, the planar coil demonstrates better performance due to the higher allowable current density of the planar coil shown in Table III. This higher current density is attributed to larger coil spacing on a polyimide substrate in the planar coil allowing for better heat dissipation.

TABLE III
SUMMARY OF VCA PERFORMANCE METRICS

	Planar Coil	Hand Wound Coil
Overall Mass	310mg	470mg
Number of turns	21	100
Stroke	4.0mm	4.0mm
Max. Force	11.8mN	59.6mN
Max. Cont. Current Density	347 A mm^{-2}	285 A mm^{-2}
Bandwidth	51Hz	55Hz
Max. Power	3.3mW	13.1mW
Power Density	1.95W kg^{-1}	6.97W kg^{-1}

Without additional spring elements, the bandwidth limit (traveling full stroke) of the planar VCA is 51Hz with a sinusoidal current input of $\pm$0.6A. The bandwidth limit of the hand-wound coil is 55Hz at $\pm$0.75A.

B. Dynamic Performance

The dynamic performance of the planar VCA is characterized by conducting a frequency sweep on the actuator. A sinusoidal current input is chosen such that minimal

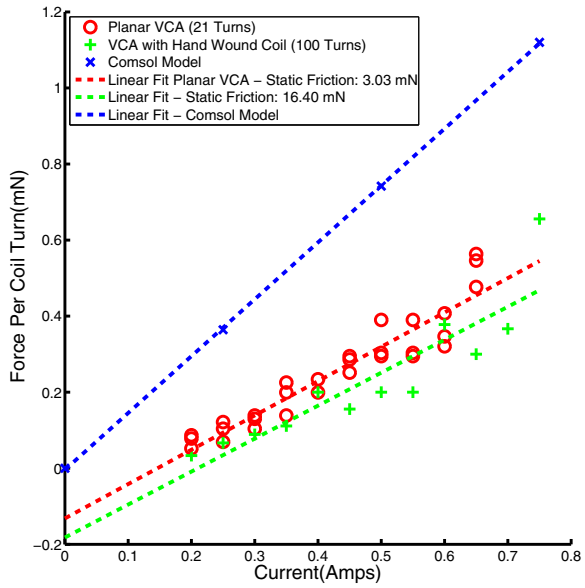

Fig. 8. Force vs. current Data for VCA with linear fit.

saturation in coil position occurs during the sweep. The raw current, force, and displacement data appears in Fig. 9.

In the bode plot in Fig. 10, there is a resonance at 20Hz with attenuation to minimal stroke amplitude after this regime. A phase offset at low frequencies is seen due to saturation of displacement in the quasi-static regime caused by frictional effects. We fit a 3rd order transfer function to the data based on the model presented in section IV-B.

$$\frac{X(s)}{I(s)} = \frac{0.2046}{3.467\times10^{-7}s^3 + 0.0022s^2 + 0.1573s + 32.64} \quad (7)$$

A 2nd order theoretical spring-mass-damper model is overlaid in Fig. 10 as an upper bound on the system with no electrical coupling ($L = k_c = 0$ in Eq. 6). The fit yields parameters $k = 2.5$, $b = 0.01$, and $m = 16\times10^{-5}$. The spring stiffness, $k = 2.5\,\mathrm{N\,m^{-1}}$, is lower than measured ($k = 5.4\,\mathrm{N\,m^{-1}}$) due to nonlinear effects at small displacements of the sarrus linkage. The damping term is low as expected due to low losses in the joints of the sarrus linkage, and the mass, $m = 16\times10^{-5}$kg, is higher than predicted ($m = 16$mg) due to mass and inertia contributions from the sarrus linkage.

VII. SUMMARY AND FUTURE WORK

We have developed a voice coil actuator that enables a new approach to actuation in mesoscale robotics. Design, modeling, methods for optimization and experiments are presented for the constructed prototypes. Measurements indicate high stroke actuation of 4mm, a bandwidth of 51Hz, and a peak force of 11.8mN. While the current prototype has a relatively low power density, initial calculations suggest the potential to reach upwards of $20\,\mathrm{W\,kg^{-1}}$ through a number of design improvements.

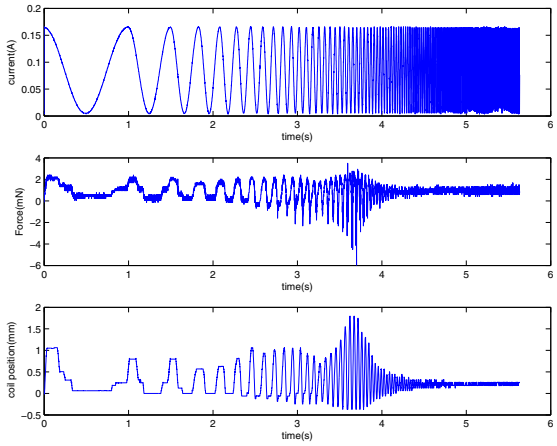

Fig. 9. Force and displacement measurements of the VCA with sarrus linkage.

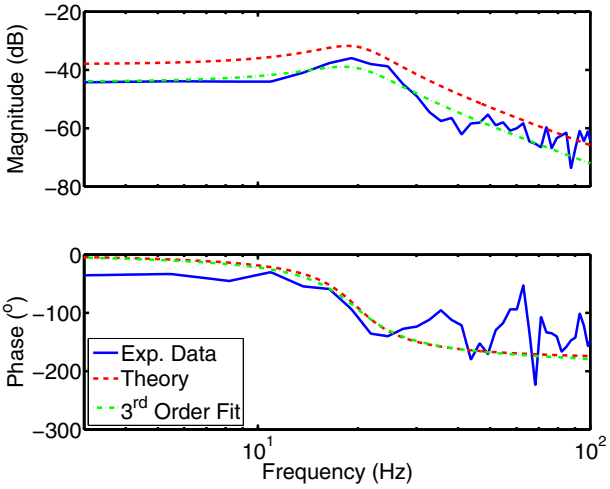

Fig. 10. Displacement vs. current bode plot of planar VCA with addition of sarrus linkage spring element.

Future designs can increase the turn density of the planar coil by improving the layer attachment and reflow process, and multi-layer windings can be fabricated using additional processing steps. The force output of the VCA can be increased by conducting a multiple-object optimization and adding a second permanent magnet on the other side of the coil, thereby using both sides of the coil for force generation. The introduction of a linear, flexure-based bearing can both improve performance and provide a convenient attachment for integrating the actuator into mesoscale robots. The VCA is suitable for many mesoscale robotics applications, and further scaling down of the actuator will be possible as the fabrication processes are refined.

ACKNOWLEDGMENTS

The authors would like to thank all Harvard Microrobotics Laboratory group members for their invaluable discussions. This work is partially funded by the Wyss Institute for

Biologically Inspired Engineering and the Army Research Labs Micro Autonomous Systems and Technology Program.

REFERENCES

[1] Maxon Motor, "Maxon EC-4pole 32mm, brushless, 480 Watt," Datasheet, June 2013.

[2] Namiki, "Micro DC Brushless Motor Series SBL02-06," Datasheet, Dec. 2011.

[3] B.R. Donald, et al. "An Untethered, Electrostatic, Globally Controllable MEMS Micro-Robot", Journal of Micromechanical Systems, Vol. 15, No. 1, Feb. 2006.

[4] Punning, Andres, et al. "A biologically inspired ray-like underwater robot with electroactive polymer pectoral fins." International IEEE Conference on Mechatronics and Robotics. Vol. 2004. 2004.

[5] M. Goldfarb, N. Celanovic, "A flexure-based gripper for small-scale manipulation", Robotica, Issue 02, March 1999.

[6] T. Ho, S. Choi, S Lee, "Development of a Biomimetic Quadruped Robot", Journal of Bionic Engineering (4) (2007) 193-199.

[7] J-S. Koh, K-J. Cho, "Omegabot: Crawling Robot Inspired by *Ascotis Selenaria*", International Conference on Robotics and Automation, 2009.

[8] A. Hoover, E. Steltz, R. Fearing, "RoACH: An autonomous 2.4g crawling hexapod robot", International Conference on Intelligent Robots and Systems, 2008.

[9] R.J. Wood, E. Steltz, and R.S. Fearing, "Optimal energy density piezoelectric bending actuators", Sensors & Actuators A: Physical 119 (2) (2005) 476-488.

[10] A. Baisch, C. Heimlich, M. Karpelson, and R.J. Wood, "HAMR3: An Autonomous 1.7g Ambulatory Robot", IEEE/RSJ International Conference on Intelligent Robots and Systems, 2011.

[11] K. Ma, P. Chirarattanon, S. Fuller, and R.J. Wood, "Controlled Flight of a Biologically Inspired, Insect-Scale Robot", Science, vol. 340, pp. 603-607, 2013.

[12] R. Kornbluh, et al. "Application of Dielectric Elastomer EAP Actuators", in *Electroactive Polymer (EAP) Actuators as Artificial Muscles: Reality, Potential, and Challenges, 2 nd ed.*, Pasadena, CA: Y. Bar-Cohen, 2004, ch. 16, sec. 1 , pp. 533.

[13] B.H. Shin, S-Y. Lee, "Micro Mobile Robots Using Electromagnetic Oscillatory Actuator", IEEE/RAS/EMBS International Con. on Biomedical Robotics and Biomechatronics, 2012.

[14] J. Zhu, et al. "Development of Electromagnetic Linear Actuators for Micro Robots", International Conference on Electrical Machines and Systems, 2008.

[15] P. Zhang, Q. Zhou "Voice Coil Based Hopping Mechanism for Microrobot", International Conference on Robotics and Automation, 2009.

[16] J. Whitney, P. Sreetharan, K. Ma, and R.J. Wood, "Pop-up book MEMS," *Journal of Micromechanics and Microengineering*, vol. 21, no. 11, p. 115021, 2011.

[17] W. Trimmer, "Microrobots and Micromechanical Systems", Sensors and Actuators, vol. 19, pp. 267-287, 1989.

[18] K & J Magnetics, *Specifications*, [Online]. Available: http://www.kjmagnetics.com/specs.asp

[19] R.J. Wood, K-J. Cho, K. Hoffman, "A novel multi-axis force sensor for microrobotics applications", Smart Materials and Structures, vol. 18, no. 12, 2009.